IEEE Access
Multidisciplinary | Rapid Review | Open Access Journal

Received January 26, 2021, accepted February 5, 2021, date of publication February 12, 2021, date of current version February 25, 2021.

Digital Object Identifier 10.1109/ACCESS.2021.3058979

A Wearable Soft Tactile Actuator With High Output Force for Fingertip Interaction

JUNG-HWAN YOUN, HEEJU MUN, AND KI-UK KYUNG, (Member, IEEE)
Department of Mechanical Engineering, Korea Advanced Institute of Science and Technology, Daejeon 34141, South Korea

Corresponding author: Ki-Uk Kyung (kyungku@kaist.ac.kr)

This work was supported in part by the Research and Development Program of National Research Foundation (NRF), South Korea, under Grant 2019R1A2C2006362, and in part by the Institute of Information and Communications Technology Planning and Evaluation (IITP) by the Korean Government through Ministry of Science and ICT (MSIT) under Grant 2020-0-00594.

ABSTRACT This paper reports a soft fingertip-mountable tactile actuator based on a Dielectric Elastomer Actuator (DEA), which exhibits high output force over a wide frequency range with a lightweight and soft structure. DEA is a soft actuator characterized by its large area strain, fast response speed, and high specific energy density. The proposed soft tactile actuator is constructed of a multi-layered conical DEA structure. This design has safety benefits because it isolates the high voltage components from the contact point. In this paper, the resonance frequency of the tactile actuator was designed to be at 250 Hz to maximize vibrotactile stimulation. In addition, the geometric design parameters of the soft tactile actuator were optimized by conducting the simulations and the experiments. Based on these efforts, the proposed actuator produces a high output force of 8.48 N at the resonance frequency, with a maximum displacement of 0.46 mm. Our wearable prototype was an entirely soft haptic system, which exhibits high output force, as well as flexibility and conformity with a total weight of 2.6 g.

INDEX TERMS Haptic interfaces, intelligent actuators, human robot interaction, soft robotics.

I. INTRODUCTION

Since the turn of a millennium, hand-held devices have become an inseparable tools in our daily lives. While these devices offer lush and vibrant visual and auditory experiences, demand is increasing for new functions, including entertainment, virtual reality, medical applications, and communication tools for blind [1]–[5]. However, there have been several attempts at enhancing hand-held haptic devices even further. Thus, the concept of wearable devices has been proposed, and tactile feedback has been implemented in wearable devices to transfer information through a new medium, i.e., the skin. So far, various wearable tactile devices have been proposed using piezoelectric actuators, cylindrical motors, servo motors, electromagnetic actuators, pneumatic or hydraulic actuators, and shape memory alloy actuators [6]–[14]. Nonetheless, to create a light-weight, flexible, and high output force tactile device especially for use in a wearable interfaces, more research needs to be done on other soft actuators.

Among many electro-active polymer (EAP) type actuators, dielectric elastomer actuators (DEAs) are promising soft actuators that are characterized by large area strain, fast response, high specific energy density, lightweight, low cost and low power consumption [15]. Because of these advantages, several researchers have proposed wearable tactile interfaces using DEAs. First, a single-layered DEA based tactile display device was presented [16]. This device can generate an output force of about 14 mN at 3.5 kV. To improve the output force performance, various DEA structures for wearable tactile devices have been introduced such as a multi-layered DEA (255 mN at 4 kV) [17], a hydro-statically coupled DEA (HCDEA) (700 mN at 4 kV) [18], [19], and a rolled DEA (1 N/cm^2 at 1 kV) [20], [21]. These previous works have shown huge improvements in the output force of DEA based tactile devices. However, for an effective tactile interface, larger output force under a wide frequency range is required.

In this paper, we present a soft finger-mountable tactile actuator based on a conical DEA structure, which is com-posed of passive/active membranes, an inner pillar, and an outer frame, as shown in Fig. 1(b). Several researchers have suggested the haptic devices based on such a conical DEA structure, but the output force of the devices (240 mN at 3.5 kV) should be enhanced for effective tactile interface [22], [23]. Although similar conical DEA structure was

The associate editor coordinating the review of this manuscript and approving it for publication was Zheng Chen.

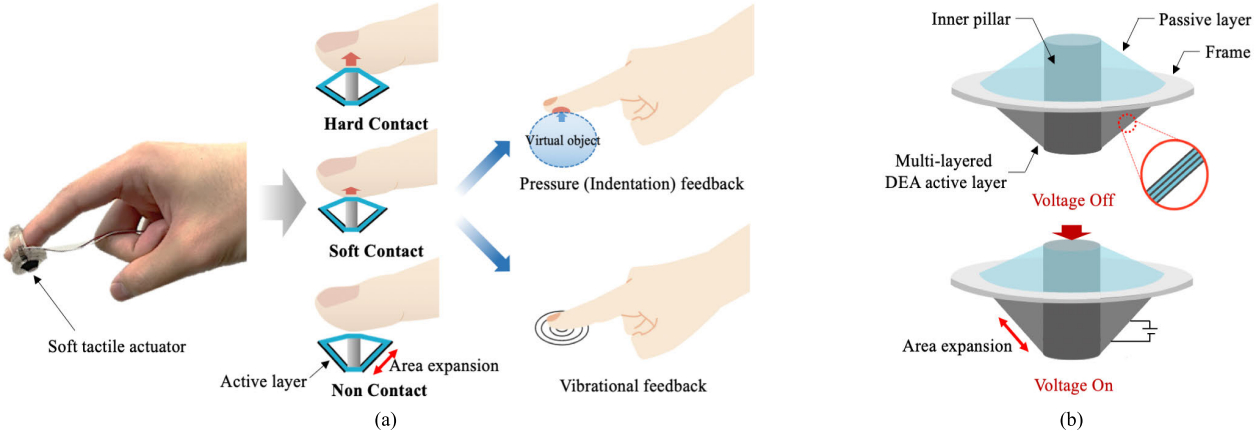

FIGURE 1. **(a) A conceptual illustration of the soft tactile actuator for providing indentation and vibrational feedback; (b) An operating principle of the soft tactile actuator under electrical stimulation producing a vertical displacement and an output force.**

used in this paper, we aimed to enhance the tactile feedback to the user by designing the soft tactile actuator as follows. First, the stiff pillar was used to deliver the output force to the user, which aims to minimize the force losses. Second, the resonance frequency of the actuator was designed to be near 250 Hz, the human fingertip region of maximum perceptual sensitivity [24]. Then, by activating the soft tactile actuator at the resonance frequency, the tactile feedback can be maximized. Lastly, we considered the size (diameter$<$15 mm, height$<$10 mm) and the weight ($<$3 g) of the actuator to enhance wearability. To meet these criteria, we optimized the dimensions of the inner pillar. The soft tactile actuator with selected design parameters was capable of producing large blocked force ($>$ 8 N) over the entire human per-ceivable frequency range of 0 to 400 Hz. In addition, the structure has advantages in terms of electrical safety because the high voltage components are totally isolated from the user's contact point. The fabricated haptic system is entirely soft, flexible, compact, and light-weight (2.6 g) making it wearable.

II. WORKING PRINCIPLE

The soft tactile actuator can apply the force feedback to the user's fingertip; this force can be controlled by the input voltage. Thanks to the compact structure and flexibility of the actuator, a soft wearable system is designed to be flexible, soft, lightweight and easy to wear. The soft tactile actuator in this research adapted the concept of a double-cone DEA [25]–[27]. The reason for choosing a double-cone DEA among various DEA configurations, is due to its high output force capability. The benefits in terms of output force of the double-cone DEA can be explained as follows. First, the proposed actuator uses both the electrostatic force of the DEA and the restoring force of the polymer. Second, the output force was transferred to the user through the stiff pillar, which can reduce the force losses and increase the bandwidth. The soft tactile actuator consists of a DEA active membrane layer and a passive membrane layer which are bonded to a circular pillar placed inside. The fingertip tactile device was fabricated by embedding a soft tactile actuator in the fingertip surface. The actuator was designed such that it can protect the user from the electric shock because high voltage parts are separated. Under zero input voltage, the soft tactile actuator presses the user's fingertip with a maximum force due to the restoring force of the polymer. When the input voltage increases, the soft tactile actuator moves downward, which leads to a decrease of the interacting force. Under the maximum applied voltage, no contact occurs between the fingertip and the actuator which provides no force to the user. It is possible to control the contact force by varying the input voltage to the actuator, as illustrated in Fig. 1(a).

The deformation of the DEA is determined by the electric field between its two electrodes of DEA [15]. When an electric field is applied to the DEA, an electrostatic pressure, known as Maxwell stress, is induced on both sides of the DEA, which leads to compression in the thickness direction. The thickness strain s_z can be expressed by a simple electrostatic model as

$$s_z = -\frac{\varepsilon_0 \varepsilon_r}{Y}\left(\frac{V}{z}\right)^2 \tag{1}$$

where V is the applied voltage, Y is the elastic modulus, ε is the relative permittivity, ε_0 is the permittivity of free space, and z is the thickness of the dielectric elastomer (DE) material [15]. Since the DE is essentially incompressible, the thickness compression leads to planar area expansion. The actuation of the soft tactile actuator depends on the force balance between the two membrane layers. Upon applying voltage to the DEA active membrane, the membrane expands in the planar direction, which causes the inner circular pillar to move downward, as shown in Fig. 1(b).

III. FABRICATION

To select the proper DE material, two different DE materials were used to fabricate the actuator. As expressed in (1), to maximize the performance of the DEA, the DE material should have low elastic modulus, high dielectric constant, low viscosity, and high electrical breakdown strength [15]. Among various DE material candidates, 3M

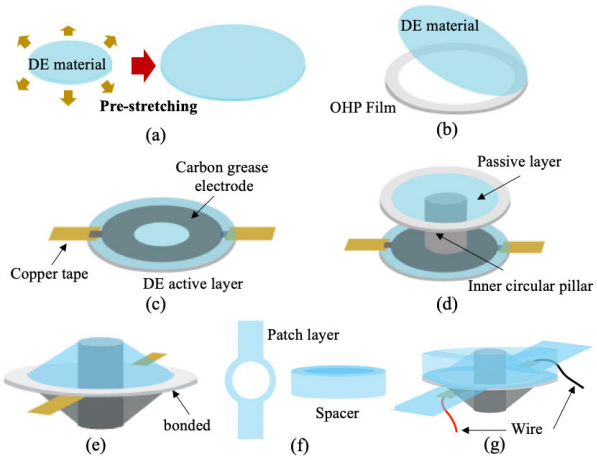

FIGURE 2. (a) Fabrication process of the soft tactile actuator: (a) Pre-stretching the DE material, (b) Attach the pre-stretched DE material to OHP film, (c) Coating with the carbon grease electrode and attach the copper tape. Repeat b-c process to make the multi-layered DEA, (d) Place a circular pillar between the two layers, (e) Fabricated soft tactile actuator, (f) fabricate the patch layer and the spacer with 3M VHB 4910 film, (g) Completed wearable tactile device.

TABLE 1. Comparison of two DE Materials [28]–[31].

Parameters	Unit	3M VHB 4905	Wacker Elastosil P7670
Young's modulus	[MPa]	0.4	0.182
Dielectric constant	[-]	4.53 @1 Hz	2.86 @10 Hz
Dielectric strength	[V/μm]	25 @0.5 mm	33 @0.1 mm

VHB 4905 acrylic elastomer and Wacker Elastosil P7670 silicone elastomer were chosen in this research. TABLE 1 compares the key parameters of the two selected DE materials [28]–[31]. It has been reported that using 3M VHB 4905 as a DE has benefits in generating a large strain under low frequency [15]. However, due to the high viscosity property of 3M VHB 4905, the silicone elastomer is preferred for high-frequency operating systems [15]. For the prototype fabrication, both the passive and active membranes were produced using DE materials which, were bi-axially pre-stretched. In this step, the commercially available 0.5 mm thick 3M VHB 4905 was pre-stretched to a ratio of 2.5. For the silicone elastomer membrane, the 0.25 mm thick blade-casted Wacker Elastosil P7670 was cured at 60°C for 4 hours. Then, the cured silicone membrane was pre-stretched to a ratio of 1.2. The difference in the thickness was due to the difference in the elastic modulus between two materials. Both pre-stretched membranes were designed to have similar nominal stiffness which can be predicted by multiplying of the elastic modulus and the thickness. To maintain the pre-strain of the membranes, the pre-stretched membranes are bonded to an Overhead Projector (OHP) film of 100 μm thickness with an outer diameter of 15 mm and an inner diameter of 12 mm. An OHP film is suitable for a soft wearable device because it is thin and flexible, but stiff enough to maintain

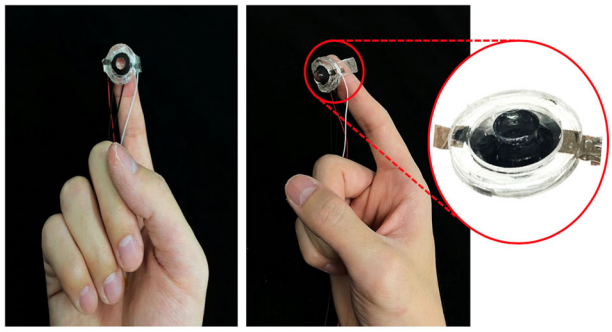

FIGURE 3. Prototype of the fingertip tactile device using the soft tactile actuator.

the pre-stretch of the membranes. The dielectric membranes were coated with carbon grease as the compliant electrode and stacked as a multi-layer structure to fabricate an active DEA membrane layer. Electrical connections were made by attaching copper tapes on both electrode surfaces of the active DEA membrane layers. Finally, an acrylic circular pillar was placed between the two layers, and two OHP films were bonded together. The wearable prototype interface comprised of the soft actuator, a patch, and a spacer as can be seen in Fig. 2. For the patch layer, 3M VHB 4910 film was chosen and bonded with polyurethane tape of 20 um thickness to remove its stickiness. The patch layer is attached to the fabricated actuator, and electrical wires are connected to the copper tapes. Finally, the spacer, made from stacked 3M VHB 4910 film, is attached to the actuator. Fig. 2 depicts the overall fabrication process of the wearable tactile device. Fingertip contact occurs in the passive membrane layer, and all high voltage components are isolated from the contact points. From the benefits of the structural design, the electrical safety can be guaranteed. The weight of the tactile actuator was 1.2 g, and the total weight of the wearable tactile device was 2.6 g. Fig.3 shows the fabricated fingertip tactile device.

IV. SIMULATION

Various dynamic models of the double-cone DEA have been presented from the previous works [25]–[27]. In this work, the Kelvin-Voigt-Maxwell based model was applied to determine the dimensions of the inner pillar to maximize the output force [26], [27]. Under the displacement of Δd, the radial strain λ_{1n} and the circumferential strain λ_{2n} of the membranes (where n = 1,2 for top membrane and bottom membrane) can be described as

$$\lambda_{11} = \frac{\sqrt{(l/2 + \Delta d)^2 + (\text{b-a})^2}}{b - a}\lambda_p \tag{2}$$

$$\lambda_{12} = \frac{\sqrt{(l/2 - \Delta d)^2 + (\text{b-a})^2}}{b - a}\lambda_p \tag{3}$$

$$\lambda_{21} = \lambda_{22} = \lambda_p \tag{4}$$

where a is the radius of the inner pillar, b is the inner radius of the circular frame, l is the height of the inner pillar, and λ_p is the pre-stretched ratio of both membranes, as in Fig. 4.

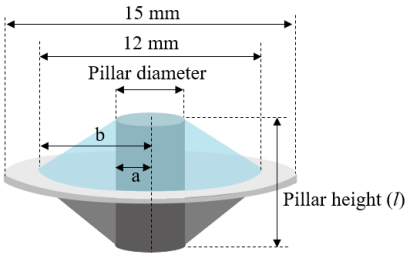

FIGURE 4. Design parameters of the soft tactile actuator.

Then, the resulting force by the tension of the membranes can be expressed as

$$m\ddot{\Delta d} = -2\pi a\frac{h_0}{\lambda_{11}\lambda_{21}}\sigma_1 \sin\alpha_1 + 2\pi a\frac{h_0}{\lambda_{12}\lambda_{22}}\sigma_2 \sin\alpha_2 - \mathrm{mg} \quad (5)$$

with

$$\alpha_1 = \tan^{-1}\left(\frac{l/2+\Delta d}{b-a}\right) \quad (6)$$

$$\alpha_2 = \tan^{-1}\left(\frac{l/2-\Delta d}{b-a}\right) \quad (7)$$

where m is the mass of the inner pillar, h_0 is the initial thick-ness of the membrane, α_n are the angle of the membranes, and σ_n are the radial stress of the membranes. The radial stress of the membranes can be determined using Kelvin-Voigt-Maxwell model as

$$\sigma_1 = \mu_1\left(\lambda_{11}^{\beta_1} - \lambda_{11}^{-\beta_1}\lambda_{21}^{-\beta_1}\right) + \mu_2\left(\lambda_{11}^{\beta_2} - \lambda_{11}^{-\beta_2}\lambda_{21}^{-\beta_2}\right) + \mu_3\left(\left(\frac{\lambda_{11}}{\xi_{11}}\right)^2 - \left(\frac{\lambda_{11}}{\xi_{11}}\right)^{-2}\left(\frac{\lambda_{21}}{\xi_{21}}\right)^{-2}\right) + \eta_2\frac{\dot{\lambda_{11}}}{\lambda_{11}} \quad (8)$$

$$\sigma_2 = \mu_1\left(\lambda_{12}^{\beta_1} - \lambda_{12}^{-\beta_1}\lambda_{22}^{-\beta_1}\right) + \mu_2\left(\lambda_{12}^{\beta_2} - \lambda_{12}^{-\beta_2}\lambda_{22}^{-\beta_2}\right) + \mu_3\left(\left(\frac{\lambda_{12}}{\xi_{12}}\right)^2 - \left(\frac{\lambda_{12}}{\xi_{12}}\right)^{-2}\left(\frac{\lambda_{22}}{\xi_{22}}\right)^{-2}\right) + \eta_2\frac{\dot{\lambda_{12}}}{\lambda_{12}} - \varepsilon_0\varepsilon_r E^2 \quad (9)$$

with

$$\frac{d\xi_{1n}}{\mathrm{dt}} = \frac{\xi_{1n}}{3\eta_1}(\mu_3\left(\left(\frac{\lambda_{1n}}{\xi_{1n}}\right)^2 - \left(\frac{\lambda_{1n}}{\xi_{1n}}\right)^{-2}\left(\frac{\lambda_{2n}}{\xi_{2n}}\right)^{-2}\right) - \mu_3\left(\left(\frac{\lambda_{2n}}{\xi_{2n}}\right)^2 - \left(\frac{\lambda_{1n}}{\xi_{1n}}\right)^{-2}\left(\frac{\lambda_{2n}}{\xi_{2n}}\right)^{-2}\right)/2) \quad (10)$$

where μ_1, μ_2, μ_3 are shear moduli, β_1, β_2 are exponent parameters, η_1, η_2 are damping coefficients, $\varepsilon_0, \varepsilon_r$ are the vacuum permittivity and the relative permittivity of DEs, E is the electric field applied to DEs, and ξ_{1n}, ξ_{2n} are the stretch of the dashpots, respectively. In the case of the proposed actuator, the upper membrane is the passive membrane, and the electric field is only applied to the bottom membrane. The details of the dynamic model of the double-cone DEA are well summarized in the previous research [25]–[27]. From the dynamic model, the displacement and the blocked force of the double-cone actuator were simulated with various pillar designs. The blocked force of the actuator is defined as an output force generated by actuator under the blocked condition. We assumed the blocked force as a tension force of the membranes under the deformation. Simulation results are plotted in Fig. 5 under the 4 kV sinusoidal input voltage at 0.1 Hz. Results showed both the displacement and the blocked force increased with the larger pillar height. However, with a larger pillar diameter, the displacement of the actuator decreased whereas the blocked force increased. It should be noticed that the inner pillar should have a large diameter and height to maximize the output force. However, the size of the actuator (height < 10 mm, diameter < 15 mm) was limited due to the consideration of wearability of the tactile device. As a result, the dimensions of the pillar was determined with a diameter of 8 mm and a height of 10 mm. With the determined pillar dimension, the effect of the number of stacked DE layers was observed based on the simulation. As can be seen in Fig. 6, by increasing the number of stacked DE layers, the output force increased, while maintaining the displacement. Thus, to maximize the output force, we choose double DEA layers.

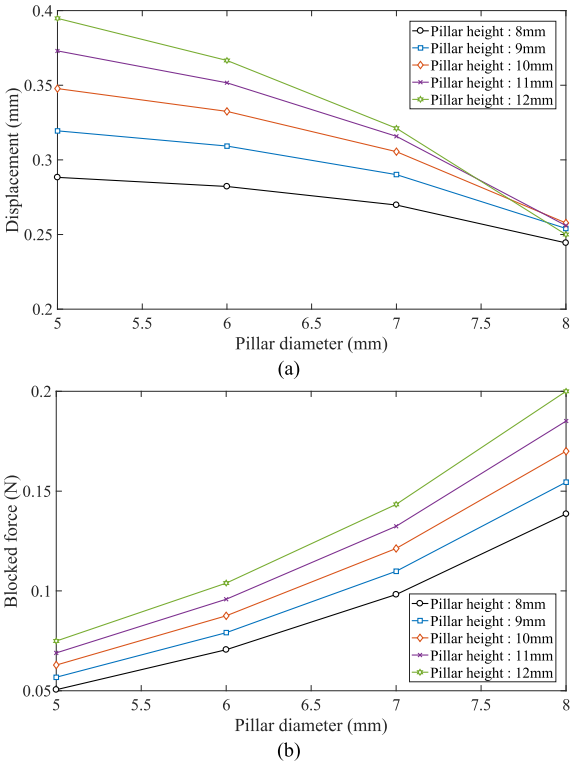

FIGURE 5. Simulation results of the various double-cone DEAs with input voltage of 4 kV (a) Maximum displacement; (b) Blocked output force.

V. DESIGN OF THE RESONANCE FREQUENCY

For an effective wearable tactile device application, the actuator needs to exert enough force and displacement. It is reported the human force perception thresholds are lowest around 250 Hz [24]. For this reason, to maximize the vibro-

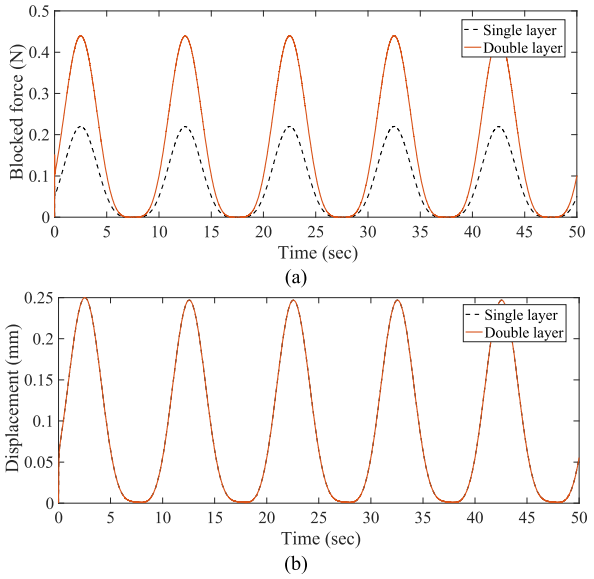

FIGURE 6. Simulation results of the double-cone DEAs with various numbers of DE layers. (a) Blocked force; (b) Output displacement.

TABLE 2. Test sample parameter of a soft tactile actuator.

Sample number	Number of stacked layers	Pillar diameter (mm)	Pillar height (mm)	DE Material
Sample 1	2	8	10	VHB 4905
Sample 2				Elastosil P7670

TABLE 3. Estimated stiffness and the design of the actuator samples.

Sample number	Estimated stiffness (N/m)	Pillar mass (g)	Inner diameter of the pillar (mm)
Sample 1	602.3	0.24	3.10
Sample 2	544.4	0.22	2.55

tactile stimulation, the resonance frequency of the actuator was designed to be at 250 Hz. Two different samples were prepared by varying the DE materials. Detailed para-meters of each sample are shown in TABLE 2. Experiments to measure the stiffness of the double-cone actuator were conducted. A 500 gf load cell (UMI-G500, DACELL) was mounted on an aluminum bracket attached to a linear stage. The linear stage moves downward at a speed of 0.1 mm/sec and simultaneously, the load cell collects the pushing force. The experimental setup is illustrated in Fig. 7(a). As the double-cone DEA was made with viscoelastic materials such as VHB 4905 or Elastosil P7670, the relationship between the dis-placement and the passive force is non-linear. However, under the small displacement (<1.5 mm), the experimental results in Fig. 7(b) show that the double-cone DEAs have an approximately linear relationship between the displacement and the passive force. This demonstrates that the quasi-stiffness of the double-cone DEAs can be considered as a constant value under 1.5 mm of displacement. TABLE 3 summarizes the estimated stiffness values of the actuator obtained by linear regression.

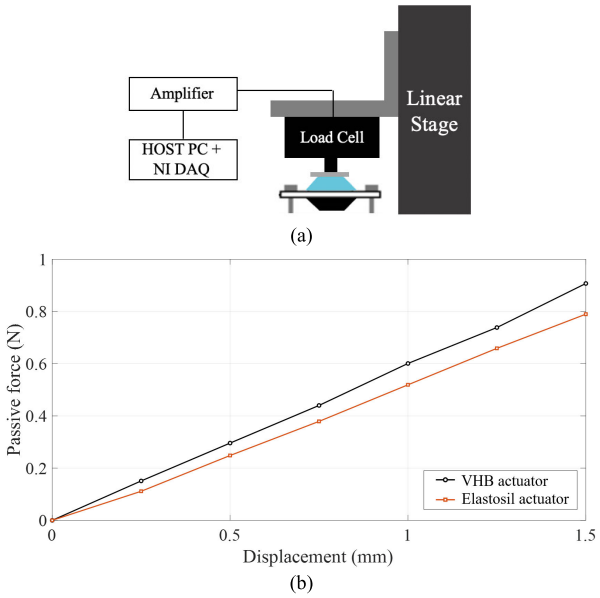

FIGURE 7. (a) Quasi-static stiffness measurement test setup; (b) Measured passive force of all samples with the measured displacement.

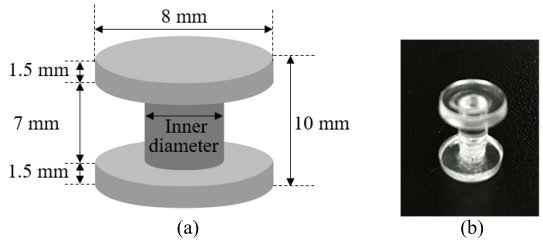

FIGURE 8. (a) Design of the inner pillar and (b) fabricated inner pillar.

To predict the resonance frequency of the double-cone DEAs, the actuator is simplified as a linear undamped oscillator [27]. The resonance frequency f_r of the actuator can be estimated from (11)

$$f_r = \frac{1}{2\pi}\sqrt{\frac{k}{m}} \tag{11}$$

where k is the estimated stiffness of the actuator, and m is the mass of the actuator. Since the weight of the membranes is negligible, the pillar mass can be determined as,

$$m_{pillar} \approx \frac{k}{4\pi^2 f_r} \tag{12}$$

To satisfy all the design requirements, the inner pillar was designed as Fig. 8. The mass of the pillar can be determined by controlling the inner diameter, as summarized in TABLE 3. As a result, the fabricated pillar is designed to have a diameter of 8 mm, a height of 10 mm, with a determined inner diameter.

VI. PERFORMANCE TEST OF SOFT TACTILE ACTUATORS

The performance of the soft tactile actuators can be evaluated by observing the displacement and output force characteristics. To measure the displacement of the

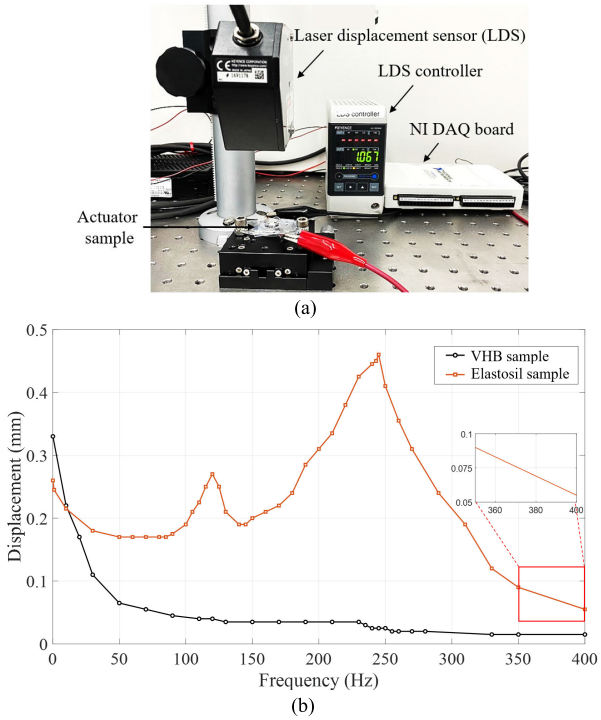

FIGURE 9. (a) Experimental setup for measuring the free displace-ment; (b) Free displacement profiles of the double-cone DEAs with the input frequency at 4 kV.

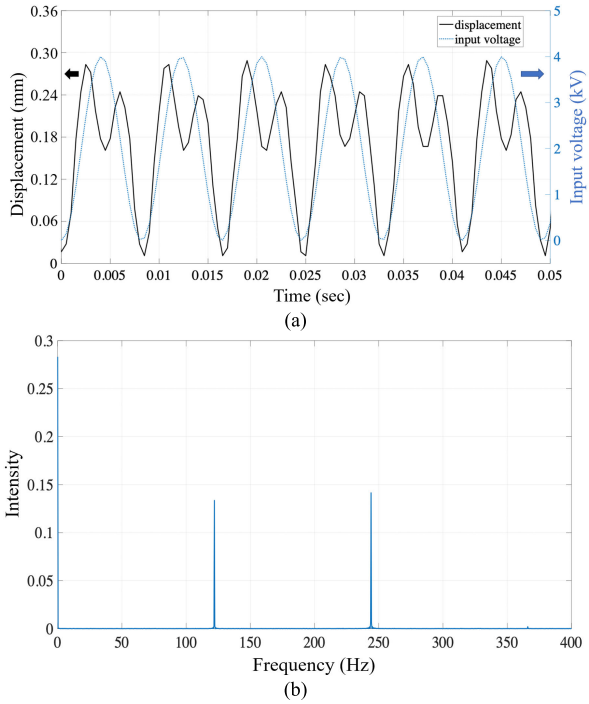

FIGURE 10. (a) Recorded displacement profile of the sample number two at 122 Hz; (b) FFT analysis of the recorded displacement signal.

actuator, a laser displacement sensor (LDS) (LK-G3000, Keyence), a high voltage amplifier (AMJ-4B10, Matsusada), a DAQ board (USB-6003, National Instruments), and a laptop were prepared. The devices were placed on top of an anti-vibration table (DVIO-I, Daeil Systems) to reduce external noise and disturbance. In this experiment, the actuator was mounted on top of a precise X-Y manual stage. The actuator's position was controlled to match the LDS's laser scanning point to the center of the actuator. The displacement measurement setup is shown in Fig. 9(a). The laptop was used to send sinusoidal voltage signals, ranging from 0.1 to 400 Hz at 4 kV to the actuator, and simultaneously to collect resulting displacement data. Results are plotted along the frequency range and are shown in Fig. 9(b). The measured displacement profiles show significant differences between the acrylic-based actuators and the silicone-based actuators. For the acrylic-based actuators, the maximum free displacements were located at 0.1 Hz. The measured free displacement of the acrylic-based actuators constantly decreased when the frequency of the input signal increased, and no resonance peaks were observed. This is due to the high viscosity of the 3M VHB 4905 acrylic elastomer [31]. For the silicone-based actuators, the resonance peaks were clearly observed in the free displacement profiles. As can be seen in the results, silicone-based actuators show two peaks. The first peak was located at half of the resonance frequency, whereas the second peak was located at the resonance frequency. To understand this harmonic mode behaviour, the displacement profile of sample number two was recorded at its first peak of 122 Hz.

As can be seen in the Fig. 10(a), the displacement profile is composed of multiple frequencies. Fig. 10(b) shows the results of Fast Fourier Transform (FFT) of the recorded displacement data. The results clearly indicate that under the input voltage of 4 kV, the dis-placement profile is composed of both 122 Hz vibration and the 245 Hz vibration, which is the resonance frequency of the actuator. This harmonic mode phenomenon commonly occurs in nonlinear oscillation. This phenomenon can be explained by the effect of V^2 term in the expression of the thickness strain of DEA, as in (1) [32]. In the low frequency range of 0 to 5 Hz, the acrylic-based actuator, shows the higher displacement performance than the silicone-based actuator. However, over the entire high frequency range of 10 to 400 Hz, the silicone-based actuator shows dis-placement performance superior to that of the acrylic-based actuator. Among samples, sample number two, which is the silicone-based actuator, shows the largest displacement (0.46 mm) at its resonance frequency of 245 Hz. The predicted resonance frequencies and measured resonance frequencies are compared in TABLE 4. The predicted resonance frequencies match well with the measured resonance frequencies with an error of 2 %. To observe the changes in surface geometry of the actuator during electrical operation, we used a 3D optical profiler (VR-5200, Keyence). As shown in Fig. 11, under input voltage of 4 kV, actuator produces a downward bulged deformation.

The performance of the actuator samples was further evaluated by observing their output force characteristics. To measure the output force of an actuator, a high voltage amplifier, a 500 gf load cell (UMI-G500, DACELL), a load

TABLE 4. Comparison of the measured resonance frequencies and the predicted resonance frequencies of the actuator Samples.

Sample number	Designed resonance frequency (Hz)	Measured resonance frequency (Hz)
Sample 1	250	-
Sample 2	250	245

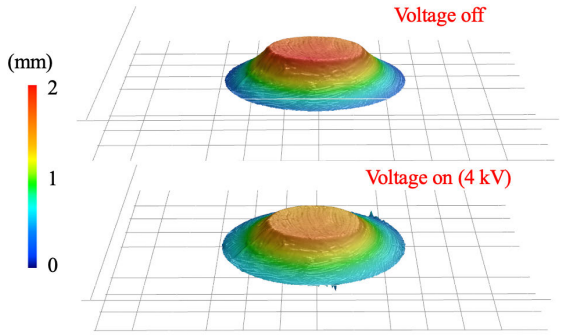

FIGURE 11. 3D surface geometry observation of the soft tactile actuator under electrical stimulation.

cell amplifier (DN-AM100, DACELL), a DAQ board (USB-6003, National Instruments), and a laptop were prepared. The devices were placed on top of an anti-vibration table, as was done in the displacement test. To ensure a precise contact between the load cell and the actuator, the load cell was connected to a linear stage. The same frequency sweep program, as used in the displacement test was used to stimulate the actuator and collect resulting load cell data. The experimental setup for the blocked force measurement is illustrated in Fig. 12(a). Blocked force measurement results are shown in Fig. 12(b). It should be noted that the actuator exerts force, in other words, pushes up, in it's off state, and retracts in its own state. Thus, for a constant force measurement, the tip of the load cell was pressed against the actuator surface. Force measurements of all samples were offset to identical initial conditions of 0.01 N at 4 kV. Similar to the displacement test results, the measured blocked force of all samples shows harmonic mode response with two peaks. The resonance frequencies of all actuator samples were located around 300∼320 Hz. Shifts in the resonance frequency of actuator samples were observed due to the effect of the loading condition. Under the low frequency range of 0 to 130 Hz, the acrylic-based actuator produces larger output force than the silicone-based actuator. However, the sample number two, which is the silicone-based actuator, showed the largest blocked force of 8.48 N at 304 Hz. The results of the maximum free displacement and the blocked force of all samples are summarized in TABLE 5. We can conclude that the acrylic-based actuators are suitable for the low frequency operating systems. However, silicone-based actuators showed superior performance in the high frequency range. Over all frequency range, actuator number two produced the largest blocked force of 8.48 N at 304 Hz, as well as the largest displacement of 0.46 mm at 245 Hz. From these results, sample actuator made with a silicone elastomer, was selected

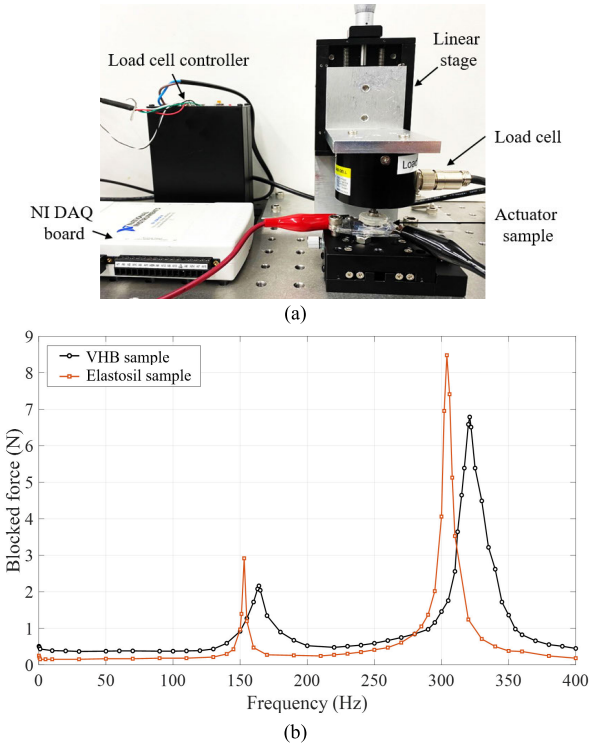

FIGURE 12. (a) Experimental setup for measuring the blocked force under the same initial loading condition; (b) Measured blocked force profiles of the actuator samples with the input frequency at 4kV.

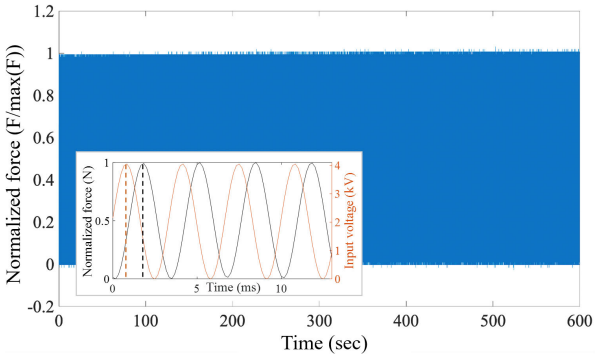

FIGURE 13. Durability test results of the soft tactile actuator.

as the soft tactile actuator. To check the durability of the selected actuator, we measured the blocked force at 304 Hz for 10 minutes. As shown in Fig. 13, the soft tactile actuator was able to produce fairly constant performance over 180,000 actuation cycles. The effects of viscoelasticity of the actuator were observed by monitoring the blocked force with respect to the input signal at the resonance frequency of 304 Hz. As shown in the inset of Fig. 13, the response follows the input signals with a small time delay of 1 ms. In addition, the viscoelastic hysteresis loops were measured at different frequencies, as shown in Fig. 14. The hysteresis loops show the relationship between the sinusoidal input voltage and the measured blocked force. The viscoelastic hysteresis is caused by the viscoelasticity of the DE material, and the viscosity of the carbon grease. The actuator showed a

TABLE 5. Experiment results of the output force and the displacement of the Four actuator samples.

Sample number	Maximum displacement (mm)	Maximum blocked force (N)
Sample 1	0.33 (@ 0.1 Hz)	6.79 (@ 321 Hz)
Sample 2	0.46 (@ 245 Hz)	8.48 (@ 304 Hz)

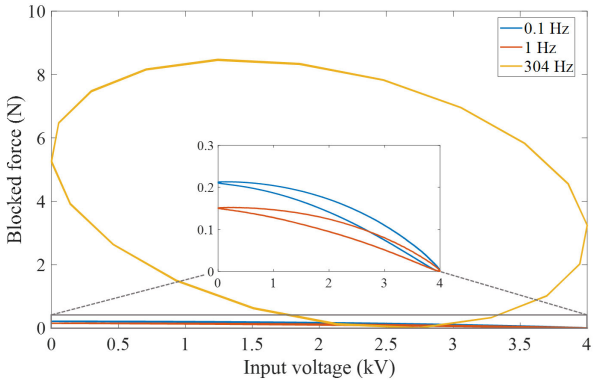

FIGURE 14. The hysteresis loops of the soft tactile actuator at different frequencies.

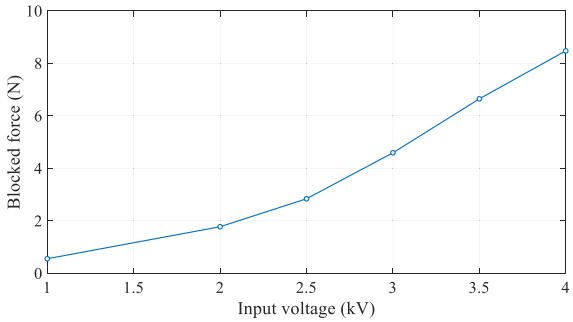

FIGURE 15. Measured blocked force (@ 304 Hz) of the selected actuator (sample number two) as a function of input voltage.

small hysteresis error of 17.21 % at 0.1 Hz. This indicates that the actuator can produce the controllable force feedback to the user. Results showed that the hysteresis errors increase with a larger operating frequency. At its resonance frequency of 304 Hz, the actuator exhibits high hysteresis error. However, it should be noted that the actuator is capable of producing large blocked force at its resonance frequency even with its large hysteresis. The blocked output force of the selected actuator was further measured as functions of the input voltage at the actuator resonance frequency. The graph in Fig. 15 shows the measured blocked force as the input voltage increased from 0 to 4 kV. It should be noted that even with an input voltage of 2 kV, the selected actuator can generate a blocked force of over 1.7 N.

The soft tactile actuator is to be worn on user's fingertip. To simulate the actual wearing condition, a skin-like soft material that has elastic properties similar to those of a fingertip was prepared. The prepared soft block, made of three layers of 3M VHB 4910 film, was attached to the tip of the load cell with the fingertip structure. The blocked forces

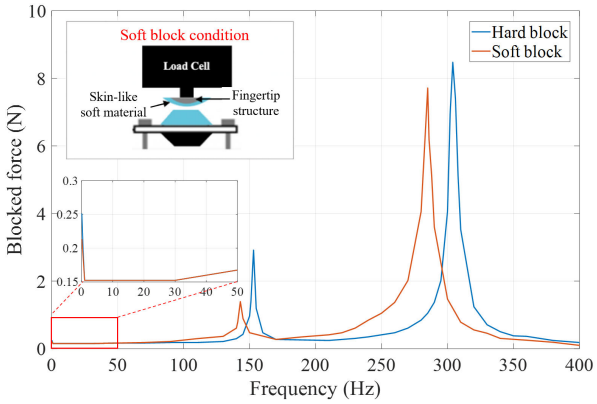

FIGURE 16. Comparison of the measured blocked force profiles of the selected actuator (sample number two) under the rigid block and the soft block condition.

under the rigid block and soft block are compared in Fig. 16. Results show that there was a decrease in the blocked force for both cases, and a shift in the resonance frequency occurred under the soft block condition. Comparing the results under the two different block conditions, the maximum blocked force de-creased from 8.48 N to 7.72 N. The resonance frequency also shifted from 304 Hz to 285 Hz under the soft block condition. We can conclude that the selected soft tactile actuator can effectively convey more than 7 N of blocked force to the user. In order to investigate the effectiveness of the proposed tactile actuator as a fingertip tactile device, we compared the performance of selected actuator with reported perception thresholds. Considering that reported force perception threshold on a fingertip was 3.9 mN at 320 Hz [24], the output force of the soft tactile actuator was more than three orders of magnitude higher at 320 Hz. As can be seen in the inset of Fig. 9(b) and inset of Fig. 16, the selected actuator was able to produce more than 0.15 N of blocked force and more than 55 μm of free displacement over the entire human perceivable frequency range of 0 to 400 Hz. Considering the previously reported displacement perception threshold, we noted that the overall displacements are larger than the perception thresholds [33]. This result indicates the proposed soft finger-mountable tactile actuator is capable of providing fairly effective force feedback to user over a wide human perceivable frequency range of 0 to 400 Hz. Another important issue is the power consumption. Our proposed DEA requires high input voltage but requires small current. The measured current flow was 0$\sim$10.46 μA during the input of 4 kV at 1 Hz. As a result, the power consumption was found to be 15.67 mW which is sufficiently small.

VII. USER TEST

To verify the usability of the proposed soft tactile actuator for fingertip interaction, the user tests were conducted with seven subjects. The age of seven subjects was between 22 to 28 years. For the preliminary test, we measured the required minimum input voltage for perceptual detection on the fingertip. The procedure for measuring the voltage

TABLE 6. Experimental results of the user tests.

Subjects	Voltage thresholds (V)		JND (%)
	Indentation feedback	Vibrotactile feedback	
Subject 1	830	460	12.0
Subject 2	670	510	11.2
Subject 3	570	370	16.1
Subject 4	570	390	11.2
Subject 5	560	290	14.9
Subject 6	630	400	14.1
Subject 7	600	270	12.7
Average	632.9	384.3	13.2

threshold is as follows. First, all subjects place their index fingertip on the actuator. Then, we apply the input voltage with different magnitudes. The input voltage is increased with a constant step of 400 V, until the participants detect the perception. Two different input voltage signals are used to detect both the indentation feedback, and the vibrotactile feedback. For the indentation feedback, square wave input voltage at 0.5 Hz is used. In the case of the vibrotactile feedback, sinusoidal input voltage at 304 Hz, which is the resonance frequency under blocked condition, is used. The experiments are repeated 4 times. Results are summarized in TABLE 6. The average voltage threshold was 632.9 V for the indentation feedback, and 384.3 V for the vibrotactile feedback. Results show that the measured voltage threshold has margin of 16.01 dB SL to maximum voltage input of 4 kV for indentation feedback, and 20.35 dB SL for vibrotactile feedback.

Next, just-noticeable-difference (JND) tests of the actuator was performed. During the test, JND of vibrotactile force was measured at 304 Hz. We test the JND at five standard stimuli [0.5, 0.51, 0.52, 0.53, 0.54] N, with a step-size of 0.01 N. To generate the selected force by actuator, the piezoelectric vibration sensor (sen-10293, Sparkfun) was attached between the actuator and subject's fingertip. Then, the voltage amplitude was selected based on the piezoelectric sensor outputs. Once the person detects the intensity change, the force difference is recoded. JND of force can be calculated as,

$$JND = \frac{\Delta F}{F} \tag{13}$$

where F is the initial force amplitude, and ΔF is the force difference when the subject detects the perceptual difference. As summarized in TABLE 6, the average of individual JNDs is 13.2%. Based on the thresholds and JND test results, we noted that the proposed actuator is capable of producing 30 steps of vibrotactile feedback at 304 Hz.

VIII. CONCLUSION

In this research, a soft finger-mountable tactile actuator was developed based on a double-cone DEA configuration. We designed the soft tactile actuator to improve the tactile feedback to the user as follows. First, the force losses were minimized as the resulting output force is transferred to the user through the stiff pillar. Second, the actuator resonance frequency was designed to be near the human maximum perceptual sensitivity at the fingertip. Lastly, the size and the weight of the actuator were limited to enhance the wearability. We optimized the design and the dimensions of the inner pillar to meet these criteria based on the simulation results and the experimental results. The selected sample was capable of producing 8.48 N of output force at 304 Hz and 0.46 mm of free displacement at 245 Hz under 4 kV input voltage. Over the entire human perceivable frequency range of 0 to 400 Hz, the output force was higher than 0.15 N. The output force of the proposed soft tactile actuator was higher than that of other DEA based tactile actuators with similar size. The effectiveness of the proposed soft actuator was investigated by conducting the user tests. Comparing with the measured voltage thresholds, the input voltage has margin of 16.01 dB SL for indentation feedback, and 20.35 dB SL for vibrotactile feedback. In addition, JND test results show that the proposed actuator is able to provide 30 steps of vibrotactile force at 304 Hz. Based on these results, it has been shown the proposed soft tactile actuator is capable of providing sufficient physical tactile feedback to the user. The entire wearable prototype interface is designed to have benefits in a compact, flexible, and light-weight structure (2.6 g). The proposed soft wearable tactile actuator can be applied in the various applications, such as virtual, augmented reality, tele-operation, and entertainments.

In the future, the performance of the soft tactile actuator will be further enhanced by improving the fabrication process and the materials. For example, we used carbon grease as compliant electrodes in this research. Using carbon grease have benefits in high conductivity, and is easy to use. However, it showed instability problem in long-term use due to the dehydration of oil. In addition, carbon grease causes the slippage issue between stacked layers, which can result inhomogeneities in the electrode coverage [34]. The high viscosity of carbon grease also effects to the dynamic response of the actuator. By using silver nanowires (Ag NWs), carbon nanotubes (CNTs), or liquid metals as complaint electrodes, these stability issues can be solved. Furthermore, the displacement of the actuator can be enhanced. In this paper, we have optimized the geometric design parameters of the actuator to maximize the output force. In the future, we will consider increasing the displacement of the actuator to provide accurate contact/non-contact tactile feedback to the user.

REFERENCES

[1] J. Minogue and M. G. Jones, "Haptics in education: Exploring an untapped sensory modality," *Rev. Educ. Res.*, vol. 76, no. 3, pp. 317–348, Sep. 2006.

[2] R. Sigrist, G. Rauter, R. Riener, and P. Wolf, "Augmented visual, auditory, haptic, and multimodal feedback in motor learning: A review," *Psychonomic Bull. Rev.*, vol. 20, no. 1, pp. 21–53, Nov. 2012.

[3] S. Jadhav, V. Kannanda, B. Kang, M. T. Tolley, and J. P. Schulze, "Soft robotic glove for kinesthetic haptic feedback in virtual reality environments," *Electron. Imag.*, vol. 2017, no. 3, pp. 19–24, Jan. 2017.
[4] E. Giannopoulos, A. Pomes, and M. Slater, "Touching the void: Exploring virtual objects through a vibrotactile glove," *Int. J. Virtual Reality*, vol. 11, no. 3, pp. 19–24, Jan. 2012.
[5] D. Escobar-Castillejos, J. Noguez, L. Neri, A. Magana, and B. Benes, "A review of simulators with haptic devices for medical training," *J. Med. Syst.*, vol. 40, no. 4, p. 104, Feb. 2016.
[6] A. M. Murray, R. L. Klatzky, and P. K. Khosla, "Psychophysical characterization and testbed validation of a wearable vibrotactile glove for telemanipulation," *Presence, Teleoperators Virtual Environ.*, vol. 12, no. 2, pp. 156–182, Apr. 2003.
[7] Y. Mo, A. Song, and H. Qin, "Analysis and performance evaluation of a 3-DOF wearable fingertip device for haptic applications," *IEEE Access*, vol. 7, pp. 170430–170441, 2019.
[8] V. Vechev, J. Zarate, D. Lindlbauer, R. Hinchet, H. Shea, and O. Hilliges, "TacTiles: Dual-mode low-power electromagnetic actuators for rendering continuous contact and spatial haptic patterns in VR," in *Proc. IEEE Conf. Virtual Reality 3D User Interfaces (VR)*, Osaka, Japan, Mar. 2019, pp. 312–320.
[9] F. Pece, J. J. Zarate, V. Vechev, N. Besse, O. Gudozhnik, H. Shea, and O. Hilliges, "MagTics: Flexible and thin form factor magnetic actuators for dynamic and wearable haptic feedback," in *Proc. 30th Annu. ACM Symp. User Interface Softw. Technol.*, New York, NY, USA, Oct. 2017, pp. 143–154.
[10] A. Talhan and S. Jeon, "Pneumatic actuation in haptic-enabled medical simulators: A review," *IEEE Access*, vol. 6, pp. 3184–3200, 2018.
[11] C. H. King, A. T. Higa, M. O. Culjat, S. H. Han, J. W. Bisley, G. P. Carman, E. Dutson, and W. S. Grundfest, "A pneumatic haptic feedback actuator array for robotic surgery or simulation," in *Proc. MMVR*, Long Beach, CA, USA, Jan. 2007, pp. 217–222.
[12] H. A. Sonar and J. Paik, "Soft pneumatic actuator skin with piezoelectric sensors for vibrotactile feedback," *Frontiers Robot. AI*, vol. 2, p. 38, Jan. 2016.
[13] H. A. Sonar, A. P. Gerratt, S. P. Lacour, and J. Paik, "Closed-loop haptic feedback control using a self-sensing soft pneumatic actuator skin," *Soft Robot.*, vol. 7, no. 1, pp. 22–29, Feb. 2020.
[14] D. Hwang, J. Lee, and K. Kim, "On the design of a miniature haptic ring for cutaneous force feedback using shape memory alloy actuators," *Smart Mater. Struct.*, vol. 26, no. 10, Sep. 2017, Art. no. 105002.
[15] J.-H. Youn, S. M. Jeong, G. Hwang, H. Kim, K. Hyeon, J. Park, and K.-U. Kyung, "Dielectric elastomer actuator for soft robotics applications and challenges," *Appl. Sci.*, vol. 10, no. 2, p. 640, Jan. 2020.
[16] H. R. Choi, D. Kim, N. H. Chuc, N. H. L. Vuong, J. Koo, J. Nam, and Y. Lee, "Development of integrated tactile display devices electroactive polymer actautors and devices," in *Proc. SPIE, EAPAD*, San Diego, CA, USA, vol. 7287, 2009, Art. no. 72871C.
[17] S. Mun, S. Yun, S. Nam, S. K. Park, S. Park, B. J. Park, J. M. Lim, and K.-U. Kyung, "Electro-active polymer based soft tactile interface for wearable devices," *IEEE Trans. Haptics*, vol. 11, no. 1, pp. 15–21, Jan. 2018.
[18] F. Carpi, G. Frediani, and D. De Rossi, "Hydrostatically coupled dielectric elastomer actuators for tactile displays and cutaneous stimulators," in *Proc. Electroactive Polym. Actuat. Devices (EAPAD)*, San Diego, CA, USA, Mar. 2010, Art. no. 76420E.
[19] H. Boys, G. Frediani, S. Poslad, J. Busfield, and F. Carpi, "A dielectric elastomer actuator-based tactile display for multiple fingertip interaction with virtual soft bodies," in *Proc. Electroactive Polym. Actuat. Devices (EAPAD)*, Portland, OR, USA, Apr. 2017, Art. no. 101632D.
[20] H. Zhao, A. M. Hussain, A. Israr, D. M. Vogt, M. Duduta, D. R. Clarke, and R. J. Wood, "A wearable soft haptic communicator based on dielectric elastomer actuators," *Soft Robot.*, vol. 7, no. 4, pp. 451–461, Aug. 2020.
[21] H. Zhao, A. M. Hussain, M. Duduta, D. M. Vogt, R. J. Wood, and D. R. Clarke, "Compact dielectric elastomer linear actuators," *Adv. Funct. Mater.*, vol. 28, no. 42, Sep. 2018, Art. no. 1804328.
[22] C. Lee, U. Kim, D.-H. Lee, C. T. Nguyen, D. T. Nguyen, H. Phung, J. Park, H. Jung, and H. R. Choi, "Development of a smart handheld surgical tool with tactile feedback," *Intell. Service Robot.*, vol. 10, no. 2, pp. 149–158, Jan. 2017.
[23] H. Phung, P. T. Hoang, C. T. Nguyen, T. Dat Nguyen, H. Jung, U. Kim, and H. R. Choi, "Interactive haptic display based on soft actuator and soft sensor," in *Proc. IEEE/RSJ Int. Conf. Intell. Robots Syst. (IROS)*, Vancouver, BC, Canada, Sep. 2017, pp. 886–891.
[24] C. Hatzfeld and R. Werthschützky, "Vibrotactile force perception thresholds at the fingertip," in *Proc. Int. Conf. EuroHaptics*. Berlin, Germany: Springer, 2010, pp. 99–104.
[25] F. Branz and A. Francesconi, "Modelling and control of double-cone dielectric elastomer actuator," *Smart Mater. Struct.*, vol. 25, no. 9, Aug. 2016, Art. no. 095040.
[26] C. Cao, X. Gao, S. Burgess, and A. T. Conn, "Power optimization of a conical dielectric elastomer actuator for resonant robotic systems," *Extreme Mech. Lett.*, vol. 35, Feb. 2020, Art. no. 100619.
[27] C. Cao, S. Burgess, and A. T. Conn, "Toward a dielectric elastomer resonator driven flapping wing micro air vehicle," *Frontiers Robot. AI*, vol. 5, p. 137, Jan. 2019.
[28] L. Liu, Y. Huang, Y. Zhang, E. Allahyarov, Z. Zhang, F. Lv, and L. Zhu, "Understanding reversible maxwellian electroactuation in a 3M VHB dielectric elastomer with prestrain," *Polymer*, vol. 144, pp. 150–158, May 2018.
[29] M. Matysek, P. Lotz, K. Flittner, and H. F. Schlaak, "High-precision characterization of dielectric elastomer stack actuators and their material parameters," in *Proc. Electroactive Polym. Actuat. Devices (EAPAD)*, vol. 6927, Mar. 2008, Art. no. 692722, doi: 10.1117/12.776177.
[30] 3M United States. (Aug. 2018). *3M VHB 4905 Technical Data Sheet*. Accessed: Jul. 15, 2020. [Online]. Available: https://3m.citrination.com/pif/000343?locale=en-US
[31] M. Zhang, "Reliability of dielectric elastomers," Ph.D. dissertation, Dept. Chem., Univ. Stuttgart, Stuttgart, Germany, 2016.
[32] S. Sasikala, K. T. Madhavan, G. Ramesh, S. Saggar, P. Predeep, and P. Chowdhury, "Electro-mechanical response to the harmonic actuation of the pneumatically coupled dielectric elastomer based actuators with and without load," *Int. J. Solids Struct.*, vols. 110–111, pp. 58–66, Apr. 2017.
[33] S. J. Bolanowski, Jr., G. A. Gescheider, R. T. Verrillo, and C. M. Checkosky, "Four channels mediate the mechanical aspects of touch," *J. Acoust. Soc. Amer.*, vol. 84, no. 5, pp. 1680–1694, Dec. 1988.
[34] P. Brochu and Q. Pei, "Advances in dielectric elastomers for actuators and artificial muscles," *Macromolecular Rapid Commun.*, vol. 31, no. 1, pp. 10–36, Jan. 2010.

JUNG-HWAN YOUN received the M.S. degree in mechanical engineering from the Yonsei University, Seoul, South Korea, in 2018. He is currently pursuing the Ph.D. degree in mechanical engineering with the Korea Advanced Institute of Science and Technology (KAIST), South Korea. In 2018, he joined the Human–Robot Interaction Laboratory, KAIST. His research interests include soft actuators, soft sensors, soft wearable robots, and haptics.

HEEJU MUN received the bachelor's degree in mechanical engineering from the Korea Advanced Institute of Science and Technology (KAIST), Daejeon, South Korea, in 2020. She is currently pursuing the master's degree in mechanical engineering. In 2020, she joined the Human–Robot Interaction Laboratory, KAIST. Her research interests include compliant sensors, soft wearable robots, and haptics.

KI-UK KYUNG (Member, IEEE) received the bachelor's and Ph.D. degrees in mechanical engineering from the Korea Advanced Institute of Science and Technology (KAIST), Daejeon, South Korea, in 1999 and 2006, respectively. In 2006, he joined the POST PC Research Group, Electronics and Telecommunications Research Institute, Daejeon, where he is currently the Director of the Smart UI/UX Device Research Section. Since 2018, he has been an Associate Professor of Mechanical Engineering and the Director of the Human–Robot Interaction Laboratory, KAIST.